

---

### Light as a material structuring tool

---

When an external electric field  $\varepsilon$  penetrates a dielectric material, ionic cores and electrons tend to separate one from another, as positive charges experience a force driving them in the direction of the field while negative charges move in the opposite direction. As a result,  $\varepsilon$  induces a local polarization of the material. Due to the mass of the ions, the movement of the ionic cores is negligible for high frequency fields and the study of the electron motion is sufficient to depict the response of the material in a good approximation.

The movement of the electrons is the result of a competition between  $\varepsilon$  and the intra atomic field  $\varepsilon_{at}$ . When  $\varepsilon \ll \varepsilon_{at}$ , the electrons experience a slight displacement before recovering their initial location. The movement of the electrons and therefore the local polarization is proportional to the electric field amplitude. Conversely, when the amplitude of  $\varepsilon$  is not totally negligible with respect to  $\varepsilon_{at}$ , the resulting polarization reads as a combination of powers of  $\varepsilon$  and nonlinear effects appear. In Sec. 2.1, we present a mathematical description of the electric field provided by an ultrafast laser source and the expression of the corresponding laser pulse intensity. Some fundamentals about the spectral properties of femtosecond pulses are also given. In Sec. 2.2, the consequences of the laser-induced nonlinear polarization on the refractive index and on the pulse propagation (self-focusing and self phase modulation) are presented.

One condition for light to become a processing tool lies in the possibility to deposit energy at chosen locations so that a threshold for material modification is surpassed. Based on this advantage, ultrafast laser irradiation has recently become a tool of choice for genuine 3D processing by confining energy deposition and restricting thermal diffusion. In order to

induce absorbance, absorption centers (e.g. free electrons) have to be created by the action of the incoming light. Section 2.3 provides a simplified discussion about laser generation of free carriers. We also describe the consequence of free carrier generation on the dielectric function of the material in the frame of the Drude model. In Sec. 2.4.1, we propose a model based on the Schrödinger equation to predict the evolution of the pulse envelope along propagation, taking into account both nonlinear effects and free carrier generation. Solving this equation provides insight into the energy deposition scheme in a transparent material.

After the laser pulse energy has been deposited into the bulk, energy relaxation processes take place. In the last section, we present the relaxation channels that have a direct consequence on the permanent refractive index of the irradiated material.

## 2.1 Mathematical description of the laser pulse

### Expression of the electric field and of the laser pulse intensity

In the following, we consider the electric field  $\varepsilon(z, r, t)$  delivered by a femtosecond laser source. The laser pulse can be described as the product of an oscillating electric field at the frequency  $\omega_0 + d\varphi(t)/dt$  with an envelope  $\bar{\varepsilon}(z, r, t)$  [11]:

$$\varepsilon(z, r, t) = \bar{\varepsilon}(z, r, t)e^{i(\omega_0 t + \varphi(t))} \quad (2.1)$$

where  $z$  corresponds to the propagation axis,  $r$  corresponds to the radial coordinates in a transverse plane with respect to the propagation axis,  $\phi$  is the relative phase and  $t$  is the time variable.

Assuming that the field envelope  $\varepsilon(r, t)$  in a plane perpendicular with respect to the propagation axis has a Gaussian temporal profile, the corresponding intensity reads:

$$I(r, t) = \frac{1}{2}cn_0\epsilon_0|\varepsilon_{ext}(r, t)|^2 = I_{max} \exp\left[-4 \ln 2 \left(r/d_{1/2}\right)^2\right] \exp\left[-4 \ln 2 \left(t/\tau\right)^2\right]. \quad (2.2)$$

The peak intensity  $I_{max}$  can be expressed as

$$I_{max} = 0.83 \frac{E}{\tau d_{1/2}^2}, \quad (2.3)$$

where  $E$  is the total pulse energy,  $d_{1/2}$  and  $\tau$  correspond to the full width at half maximum (FWHM) of the spatial and temporal intensity distributions, respectively. It is sometimes more convenient to characterize the size of the beam with respect to  $w$ , the radius at which the intensity drops by  $1/e^2$ . The relationship between  $d_{1/2}$  and  $w$  is given by

$$w = \frac{d_{1/2}}{\sqrt{2 \ln 2}}. \quad (2.4)$$

In Eq. 2.2, the dependence of the pulse profile along the  $z$  axis is not treated. In the frame of our experiment, the evolution of the pulse along the propagation axis is determined by the focusing conditions. This aspect is detailed in Sec. 3.2.1.

### Spectral properties

Assuming constant spatial phase, the spectral expression of the pulse  $\varepsilon(\omega)$  is related to  $\varepsilon(t)$  through a Fourier transform according to

$$\varepsilon(\omega) = \mathcal{F}\{\varepsilon(t)\} = \int_{-\infty}^{+\infty} \varepsilon(t)e^{-i\omega t} dt = \bar{\varepsilon}(\omega)e^{i\Phi(\omega)}, \quad (2.5)$$

where  $\bar{\varepsilon}(\omega)$  and  $\Phi(\omega)$  correspond to the pulse spectral amplitude and spectral phase, respectively. As a result, the pulse duration  $\tau$  and the FWHM of the laser pulse spectrum  $\Delta\omega$  are not independent [11], and

$$\Delta\omega\tau \geq 2\pi c_B, \quad (2.6)$$

where  $c_B$  is a coefficient depending on the pulse shape. The laser sources used in this thesis (see Tab. 3.1) are assumed to deliver Gaussian pulses for which  $c_B = 0.441$ .

For  $\Delta\omega\tau = 2\pi c_B$ , the pulse is Fourier limited and exhibits the shortest pulse duration. All the different spectral components are in phase at the center of the pulse. When the different spectral components are out of phase,  $\omega_0 + d\varphi(t)/dt = f(t)$  and the pulse is said to be chirped. A linear chirp (i.e.,  $f(t) = at$ ) corresponds to a simple pulse broadening. With the help of a pulse shaping apparatus, it is possible to intervene selectively on the respective time delays between the different spectral components by affecting the spectral phase  $\Phi(\omega)$ , in order to reach arbitrary pulse shapes. This point will be further detailed in Sec. 3.1.2.

## 2.2 Nonlinear propagation

The pulse propagation in a dielectric medium depends on the spatial and temporal characteristics of intensity and on the self-action exercised by nonlinear coupling between light and matter. Some of the factors affecting propagation are given below. The pulse propagation in a dielectric medium depends on the spatial and temporal characteristics of intensity and on the self-action exercised by nonlinear coupling between light and matter. Some of the factors affecting propagation are given below

### 2.2.1 Origin of the nonlinear refractive index

At the laser intensities used in our experiments ( $\sim 10^{13}$  W.cm<sup>-2</sup>), it is adequate to describe the nonlinear polarization as a combination of terms up to the third power of the electric

field only. In a material with an inversion symmetry,  $\chi^{(2)} = 0$  and the nonlinear polarization  $P_{NL}$  can be expressed as [12]:

$$P_{NL} = \epsilon_0 \left[ \chi^{(1)} + \frac{3}{4} \chi^{(3)} |\epsilon_{ext}|^2 \right] \epsilon_{ext} \quad (2.7)$$

where  $\chi^{(m)}$  is the  $m$ -th order susceptibility of the material. Whenever the linear absorption can be neglected, the corresponding refractive index  $n$  reads [12, 13]

$$n = \sqrt{1 + \chi^{(1)} + \frac{3}{4} \chi^{(3)} |\epsilon_{ext}|^2} = n_0 \sqrt{1 + \frac{3}{4n_0^2} \chi^{(3)} |\epsilon_{ext}|^2}. \quad (2.8)$$

Considering that the nonlinear term is small compared to the linear susceptibility, the last equation can be rewritten as :

$$n = n_0 \left( 1 + \frac{3\chi^{(3)}}{4n_0^3 \epsilon_0 c} \frac{1}{2} c n_0 \epsilon_0 |\epsilon_{ext}|^2 \right) = n_0 + n_2 I, \quad (2.9)$$

leading to a dependence of the refractive index on the laser pulse intensity (Kerr effect). The nonlinear refractive index  $n_2$  is related to the third order material susceptibility  $\chi^{(3)}$  and to  $n_0$  by

$$n_2 = \frac{3\chi^3}{4\epsilon_0 c n_0^2} \quad (2.10)$$

and has typically values making it negligible at low intensities. For instance,  $n_2 = 2.48 \times 10^{-16} \text{cm}^2/\text{W}$  in fused silica [14]. Equation 2.9 shows the importance of the laser intensity  $I(r, t)$ , defined by Eq. 2.2, as the refractive index seen by the pulse follows the local and temporal intensity profile. In our experimental conditions, the spatio-temporal dependence of the refractive index results in dramatic alterations of the spatial phase (self-focusing) and of the temporal phase (self-phase modulation) of the incoming pulse.

### 2.2.2 Self-focusing

Qualitatively, the spatial Gaussian profile of the beam involves a Gaussian refractive index profile. It results in a lens-like response of the media, provoking an auto-induced collapse of the incident beam and preventing further propagation [15]. This beam self-trapping occurs for a critical power given by [16]

$$P_{cr} = \eta \left( \frac{\lambda^2}{4\pi n_0 n_2} \right) \quad (2.11)$$

where  $\lambda$  is the wavelength of the beam and  $\eta$  is a constant independent of the material. The value

$$\eta = \frac{1.22\pi^2}{8} \quad (2.12)$$

given in [17] is generally adopted. Interestingly, the threshold for self-focusing depends on the peak power and not on the laser intensity. As explained in [13], this happens because an increase in the size of the beam translates in a smaller refractive index change which is compensated by a variation in the area of the self-focusing lens. Those two effects balance and result in a refractive power of similar amplitude, despite of the drop of the local intensity.

In fused silica, at a 800 nm wavelength,  $n_0 = 1.453$ ,  $n_2 = 2.48 \times 10^{-16} \text{cm}^2/\text{W}$  and the critical power for self focusing  $P_{cr} = 2.1 \text{ MW}$ . For a 100 fs pulse duration, this threshold is reached for a laser pulse energy higher than  $0.2 \mu\text{J}$ . Practically, whereas the laser pulse energy we normally use (typically between  $0.2$  and  $10 \mu\text{J}$ ) results in peak powers exceeding the self-focusing critical power, beam self-trapping and catastrophic collapse do not occur in our experiments, due to the consequences of free carriers generation which arrests the collapse due to plasma defocusing [18]. For a converging beam, the self-focusing contribution comes in addition to the external focusing and results in a displacement of the focal point toward the laser [19]. When dealing with pulses of light, this displacement varies in time with the instantaneous intensity of the pulse and results in a moving focal point [20]. In the case of weak self-focusing, i.e. when the peak power is less than a quarter of the critical beam power, the influence of the self-focusing on the transverse dimension of the beam leads to an increase of the intensity (see for instance [21] and references therein)

$$I_{sf} = \frac{I}{1 - \frac{P}{P_{cr}}}, \quad (2.13)$$

where  $I$  is the intensity in absence of self-focusing (see Eq. 2.2).

### 2.2.3 Self-phase modulation

As mentioned in [13], self-phase modulation is the counterpart of self-focusing in the temporal domain. Self-phase modulation is due to the time dependence of the beam intensity provoking a temporal dependence of the refractive index. The propagation through a length  $L$  translates to a phase

$$\varphi = kL - \omega_0 t = \frac{2\pi}{\lambda_0} n(I)L - \omega_0 t, \quad (2.14)$$

where  $\omega_0$  and  $\lambda_0$  are the carrier frequency and the central wavelength, respectively, of the pulse in vacuum. Remembering that the instantaneous frequency  $\omega_{inst}$  and the phase are related through

$$\omega_{inst} = -\frac{d\varphi}{dt}, \quad (2.15)$$

by differentiating Eq. 2.14  $\omega$  finally writes

$$\omega = \omega_0 + \frac{2\pi L}{\lambda_0} \frac{dn(I)}{dt} = \omega_0 + \frac{4\pi L I_0 n_2}{\lambda_0 \tau^2} t \exp\left(-\frac{t^2}{\tau^2}\right). \quad (2.16)$$

From the last equation, it appears that the leading edge of the pulse (for  $t < 0$ ) shifts to lower frequencies while the trailing edge shifts to higher frequencies in a symmetrical fashion. As a main result, new frequencies are generated in the pulse spectrum upon nonlinear propagation with consequences on the temporal shape.

## 2.3 Nonlinear ionization and consequences on the transient optical properties

Under the action of the laser pulse the material starts absorbing radiation and an excited state of matter is created. In this section, we present a review of the ionization mechanisms.

### 2.3.1 Nonlinear ionization mechanisms

#### Laser generation of free carriers at high intensities

The interaction between the electronic system and the incident electromagnetic wave is of primary importance and determines whether light is allowed to propagate in a material or not. In dielectrics, electrons are strongly bound to the lattice, precluding a possible interaction with incoming light. The minimum energy needed to free electrons from the atomic system (binding of 7.5 to 10 eV for fused silica) is well above the photon energy of the infrared light source used for irradiation (ca. 1.55 eV). Hence, infrared light is expected to propagate through a perfect crystalline transparent target without attenuation. Nevertheless, at higher intensities multiphoton ionization (MPI) is possible with a probability per time unit depending on the intensity  $I$  of the irradiating source

$$W_{PI}(I) = \sigma_K \left( \frac{I}{\hbar\omega} \right)^K \quad (2.17)$$

for a single bound electron to absorb simultaneously  $K$  photons of energy  $\hbar\omega$ . Here,  $\sigma_K$  is the  $K$ -photon absorption coefficient, called "generalized multiphoton absorption cross-section". It defines the probability that  $K$  photons find themselves simultaneously at the same location to interact with a reservoir of collision partners. The number of photons ( $K$ ) of energy  $\hbar\omega$  needed to promote an electron from the valence band into the conduction band is so that  $K\hbar\omega \geq E_{crit}$  with

$$E_{crit} = E_g + E_{osc} = E_g + \frac{e^2\epsilon_0}{2cn_0m_{opt}\omega_0^2}, \quad (2.18)$$

where  $m_{opt}$  is the electron optical mass,  $E_g$  is the band gap of the target material and  $E_{osc}$  corresponds to the oscillation energy. Typically, in fused silica, for a 800 nm wavelength,  $K$  is about 6. The multiphoton ionization rate dependence on the 6<sup>th</sup> power of  $I$  explicitly shows the nonlinear character of the interaction and hence the high intensity sensitivity of this process.

When the laser intensity is sufficiently high, the laser generation of free carriers is described using the concept of tunneling ionization. Under the influence of a very intense external electric field, the depth of the Coulomb well binding an electron to its atom is significantly reduced. By tunnel effect, the initially bound electron can cross the remaining potential barrier and free itself from the atom attraction.

Free carrier generation in intense laser fields can be treated in a unified conceptual framework according to the Keldysh model [22]. Depending on the value of the Keldysh parameter  $\gamma$  [22], it is more adequate to consider MPI, tunneling, or an intermediate model. This parameter, also called adiabatic parameter, reads [23]

$$\gamma = \frac{\omega}{e} \left[ \frac{m_{opt} c n \epsilon_0 E_g}{2I} \right]^{\frac{1}{2}}. \quad (2.19)$$

In this equation,  $\omega$  is the excitation frequency,  $m_{opt}$  and  $e$  are the reduced mass and charge of the electron, respectively,  $c$  is the velocity of light,  $n$  is the refractive index of the material,  $\epsilon_0$  is the free space permittivity, and  $E_g$  is the bandgap of the target material.

Given the critical role of the laser intensity  $I$ , defined in Eq. 2.2, proper care has to be taken in that concerns the energetic and the focusing conditions.

In fused silica ([23]), when  $\gamma \gg 1$ , MPI dominates and when  $\gamma \ll 1$ , the photoionization is properly described by tunneling.  $\gamma \approx 1$  corresponds to an intermediate situation. In fused silica ( $E_g = 8$  eV,  $n = 1.453$  at a wavelength of 800 nm), taking  $m_{opt}$  equal to the free electron mass for simplicity,  $\gamma = 1$  for a laser pulse intensity  $I \approx 5 \times 10^{13}$  W/cm<sup>2</sup>. According to Couairon et al. [23] who worked in focusing conditions comparable to ours [23],  $I$  reaches this value near the focus for a laser pulse energy of 1  $\mu$ J.

The Keldysh model is often criticized, because the prediction of the damage thresholds does not match the experimental observations over a broad range of pulse durations [24]. However, in absence of an alternative unified frame of description, this model is still widely used.

### Collisional ionization

Photo-generated free carriers are injected in the conduction band with a kinetic energy  $E_{kinetic} = K E_{photon} - E_{gap}$ .

Additionally, free electrons can also gain energy by absorbing photons due to inverse bremsstrahlung (see Eq. 2.31). If the energy surplus exceeds the ionization potential, a new electron can be promoted into the conduction band by electron impact ionization. As a result, two electrons close to the bottom of the conduction band are created. The change of electron density in the conduction band is proportional to the amount of seed electrons  $N_e(t)$  and to the laser intensity  $I(t)$  defined in Eq. 2.2 according to [25]

$$\frac{dN_e}{dt} = \alpha I(t) N_e(t). \quad (2.20)$$

### Interdependence between MPI and impact ionization

At regimes where tunneling ionization is not preponderant, multiphoton ionization (MPI) and collisional processes (avalanche) determine the free carrier generation. Stuart *et al.* [25] proposed a simple rate equation in order to describe free carrier generation, taking into account both avalanche and MPI:

$$\frac{dN_e}{dt} = \alpha I(t) N_e(t) + W_{PI}(I)(N_0 - N_e), \quad (2.21)$$

where  $I(t)$  is the intensity of the laser pulse,  $\alpha$  is the avalanche coefficient,  $W_{PI}$  is the probability per time unit of the  $K$ -multiphoton process defined in Eq. 2.17,  $N_0$  and  $N_e$  are the density of atoms and the density of free carriers, respectively, assuming that each atom provides a single free electron. In this model, seed electrons needed to trigger avalanche multiplication are supplied by multiphoton ionization. The rate of free carrier generation by avalanche depends on the total number of free carriers created by both MPI and previous collisional processes at time  $t$  and evolves linearly with  $I$ ,  $\alpha$  being quasi independent on  $I$ . This linearity holds only under the flux doubling condition, which states that as soon as an electron has enough energy to ionize a carrier from the valence band, it does so.

A correction of this model has been proposed recently by B. Rethfeld [26]. For energy and momentum conservation reasons, only the electrons with a critical energy exceeding the ionization potential by a factor of 1.5 (in a simplified case where the optical mass of the electrons in the valence and in the conduction band are equal to the free electron mass) contribute to collisional ionization [27]. Because of the non stationary energy distribution of the free electronic population on ultrashort timescales, collisional ionization actually plays a minor role at short pulse durations. As a confirmation, direct measurements of the free carrier densities around the damage threshold in  $\text{SiO}_2$ ,  $\text{MgO}$  and  $\text{Al}_2\text{O}_3$  emphasized the limited role of avalanche phenomena for short duration laser pulses [28, 29].



### 2.3.2 Optical properties of an excited solid

We explained in the previous sections how electrons could be injected in the conduction band by an intense light source. The optical properties of a material depending on the behavior of the free electrons when irradiated with an electromagnetic wave, as a consequence of their finite mass and ability to follow field oscillations [30], the generation of free electrons translates into an alteration of the complex refractive index  $\hat{n}^2$  according to [31]

$$\hat{n}^2 = \epsilon^* = \epsilon_g + \Delta\epsilon_{fcr} \quad (2.22)$$

where  $\epsilon_g$  is the initial dielectric constant of the material and  $\Delta\epsilon_{fcr}$  is the change in of the dielectric constant due to the free carrier generation.

#### Expression of the refractive index of an excited dielectric solid

The following discussion focuses on the determination of  $\hat{n}^2 = \epsilon^*$  of an excited solid, complex quantity determined by its real part  $n^*$  and its imaginary part, also known as the extinction coefficient,  $\kappa^*$ .

In the frame of the Drude model, considering that the free carrier absorption can be assimilated to the free electron absorption only (i.e. the contribution of the holes is neglected), the complex dielectric constant  $\epsilon^*$  reads (see [32])

$$\epsilon^* = \epsilon_1 + i\epsilon_2 = \epsilon_g - \left(\frac{\omega_p}{\omega}\right)^2 \frac{(\omega t_D)^2}{1 + (\omega t_D)^2} + i \left(\frac{\omega_p}{\omega}\right)^2 \frac{\omega t_D}{1 + (\omega t_D)^2} \quad (2.23)$$

where  $t_D$  is the phenomenological Drude scattering time (a measure of dephasing by elastic collisions) and  $\omega_p$  is the plasma frequency, depending on the electron density  $N_e$  and on the free electron optical mass  $m_{opt}$  according to

$$\omega_p = \sqrt{\frac{N_e e^2}{\epsilon_0 m_{opt}}}. \quad (2.24)$$

In the last expression,  $e$  is the electron charge and  $\epsilon_0$  is the vacuum permittivity. The intuitive concept of critical density refers to the special case where the electron density  $N_e = N_{cr}$  so that  $\omega_p$  is equal to the laser frequency  $\omega_0$ . From Eq. 2.24,

$$N_{cr} = \frac{\omega_0^2 \epsilon_0 m_{opt}}{e^2}. \quad (2.25)$$

Using the relations

$$\epsilon_1 = n^{*2} - \kappa^{*2} \quad \text{and} \quad \epsilon_2 = 2n^* \kappa^* \quad (2.26)$$

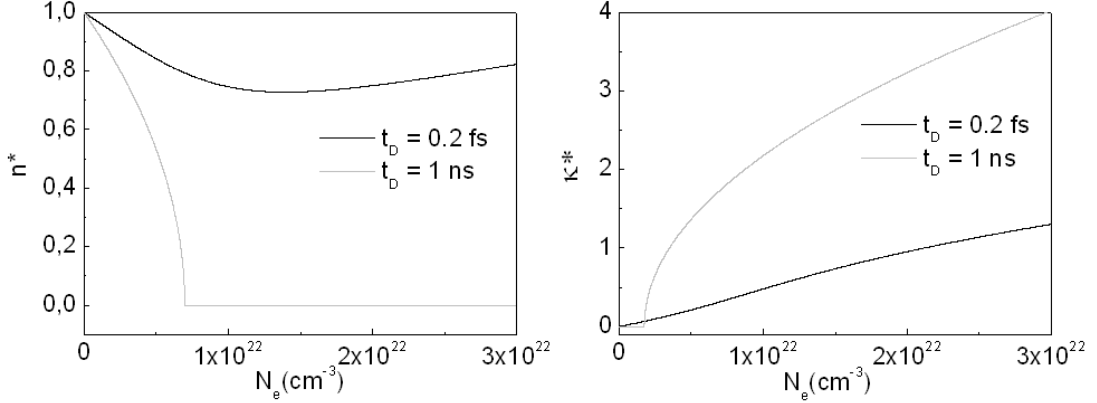


Figure 2.1: Evolution of the real part of the refractive index ( $n^*$ ) and of the extinction coefficient ( $\kappa^*$ ) of a free electron gas in vacuum versus the density of free carriers, for an incident monochromatic wave with a wavelength of 400 nm. In order to illustrate the influence of the collision parameter, computations were carried out for  $t_D = 0.2$  fs and  $t_D = 1$  ns.

gives for  $n^{*2}$  and  $\kappa^{*2}$

$$n^* = \sqrt{\frac{1}{2} \left( \sqrt{\epsilon_1^2 + \epsilon_2^2} + \epsilon_1 \right)} \quad \text{and} \quad \kappa^* = \sqrt{\frac{1}{2} \left( \sqrt{\epsilon_1^2 + \epsilon_2^2} - \epsilon_1 \right)}. \quad (2.27)$$

In Fig. 2.1 we show the evolution of  $n^*$  versus the density of the free electron gas  $N_e$  in vacuum ( $\epsilon_g = 1$ ,  $m_{opt} = m_e$ ) for  $t_D = 0.2$  fs and  $t_D = 1$  ns, in order to illustrate the importance of the phenomenological collision rate. The results presented have been computed for an incident monochromatic wave with a wavelength of 400 nm. Noticeably, for high densities and high values of  $t_D$ ,  $n^*$  goes to zero, meaning that light is not allowed to propagate in a free electron gas with a low collision rate above the critical density  $N_{cr} \approx 7 \times 10^{21}$   $\text{cm}^{-3}$  for an incident laser light at a wavelength of 400 nm (see Eq. 2.25). All the energy of the incident wave is then absorbed and/or reflected. This behavior is very similar to the behavior of a metal and therefore, such a free electron gas (with a low collision rate) is said to be in a metallic state.

When  $n^*$  stays close to one, e.g. for small values of  $t_D$ ,  $\kappa^*$  is proportional to  $N_e$  and is given by

$$\kappa^* = \frac{\omega_p^2 t_D}{2\omega(1 + \omega^2 t_D^2)} = N_e \frac{e^2 t_D}{2\epsilon_0 m_e \omega (1 + \omega^2 t_D^2)}. \quad (2.28)$$

Figure 2.1 confirms that this approximation is only valid for small values of  $t_D$ .

### Absorbance of a free electron gas

When propagating through an electron gas of density  $N_e$ , an electromagnetic wave of intensity  $I_0$  experiences a partial absorption due to inverse bremsstrahlung. We briefly mention

that inverse bremsstrahlung is a 3-body collisional process (for momentum and energy conservation reasons) in which a free electron absorbs a photon in the presence of a scattering center and consequently increases its kinetic energy. The output intensity  $I$  can be expressed by applying the Beer-Lambert law. In the case of light propagation through a  $L$ -thick electron gas, the Beer-Lambert law reads

$$I = I_0 \exp(-AL), \quad (2.29)$$

where  $A$  is the absorbance of the electron gas, related to the extinction coefficient  $\kappa^*$  via

$$\kappa^* = \frac{\lambda}{4\pi} A. \quad (2.30)$$

The combination of Eq. 2.30 and Eq. 2.28 provides a direct relation between  $N_e$  and  $A$  according to

$$A = \frac{ke^2 t_D}{m_{opt} \epsilon_0 \omega (1 + \omega^2 t_D^2)} N_e = \sigma N_e, \quad (2.31)$$

where  $k = 2\pi/\lambda$  is the wave number of the incident light and  $\sigma$  corresponds to the cross-section for inverse bremsstrahlung.

### 2.3.3 Plasma defocusing

In Sec. 2.3.1 we saw that the high intensities reached upon beam focusing allowed to generate a population of free electrons via MPI and subsequent collisional processes. We highlighted that the ionization processes were nonlinear, i.e. they depend on the intensity of the beam. Therefore, the density of free carriers follows the intensity profile of the pulse. In Sec. 2.3.2, the complex refractive index of an electron gas was studied. Remarkably, we emphasized that the real part of the refractive index decreases when the density of free electrons increases.

When an intense laser beam propagates in a transparent medium, both effects conjugate and result in the onset of a transient divergent lens upon laser action due to the non-uniform spatial profile of intensity. This mechanism drastically affects the beam propagation and competes with self-focusing (see Sec. 2.2.2). Plasma defocusing and self-focusing balance for free carriers densities  $N_e$  of less than  $10^{17} \text{cm}^{-3}$  [33], and a filamentation process can take place.

## 2.4 Pulse propagation and energy deposition

### 2.4.1 Evolution of the pulse envelope

We now present a model predicting the effects of nonlinear propagation on the temporal and spatial characteristics of the pulse envelope  $\bar{\epsilon}$  along the  $z$  axis [23]. This model is well

adapted to moderated input energies within the paraxial approximation. The encoding, computation, and presentation of the results have been derived within the frame of a cooperation project with Institute of Thermophysics (I. Burakov), and have been published in part [34, 35]. Without entering into details which can be found elsewhere and notably in [36, 23], we solve the optical nonlinear Schrödinger equation which describes pulse evolution during propagation in a nonlinear medium:

$$\begin{aligned} \frac{\partial \bar{\varepsilon}}{\partial z} = & \frac{i}{2k} T^{-1} \left( \frac{\partial^2}{\partial r^2} + \frac{1}{r} \frac{\partial}{\partial r} \right) \bar{\varepsilon} - \frac{ik''}{2} \frac{\partial^2 \bar{\varepsilon}}{\partial t^2} \\ & + \frac{ikn_2 T}{n_0} \left[ (1 - f_R) |\bar{\varepsilon}|^2 + f_R \int_{-\infty}^t dt' R(t - t') |\bar{\varepsilon}|^2 \right] \bar{\varepsilon} \\ & - \frac{\sigma}{2n_0^2} (1 + i\omega_0 t_D) T^{-1} (N_e \bar{\varepsilon}) - \frac{1}{2} \frac{W_{PI}(|\bar{\varepsilon}|) E_{crit}}{|\bar{\varepsilon}|^2} \bar{\varepsilon}. \end{aligned} \quad (2.32)$$

The first term accounts for diffraction in the propagation media in cylindrical coordinates and the second term corresponds to the group velocity dispersion, characterized by  $k''$ . The nonlinear part of the propagation due to the phenomena detailed in Sec. 2.2 is taken into account in the third term including the  $n_2$  factor. The following term deals with the absorption and defocusing of the electronic plasma (cf. Sec. 2.3.2 and Sec. 2.3.3). It includes the free carrier inverse bremsstrahlung cross section  $\sigma$  defined within the Drude formalism (see Eq. 2.31) and the last term accounts for the energy absorption due to photoionization (cf. Sec. 2.3.1). The operator  $T$  is defined as

$$T = 1 + \frac{i}{\omega_0} \frac{\partial}{\partial t} \quad (2.33)$$

and accounts for the spatio-temporal coupling.  $T^{-1}$  in front of the transverse Laplacian corresponds to space-time focusing and  $T$  in front of the term containing the nonlinear refractive index corresponds to self-steepening. Self-steepening is a consequence of the phase velocity dependence on the laser intensity, leading to a dramatic alteration of the pulse envelope.

## 2.4.2 Continuity equation

Equation 2.32 is coupled to the evolution of the free carriers density. The continuity equation reads as

$$\frac{\partial N_e}{\partial t} = \left[ W_{PI}(|\bar{\varepsilon}|) + \frac{\sigma N_e / N_0}{n_0^2 \left( 1 + \frac{m_{opt}}{m_e} \right) E_{crit}} |\bar{\varepsilon}|^2 \right] (N_0 - N_e) - \frac{N_e}{t_{tr}}. \quad (2.34)$$

The first term of the right member accounts for free electron generation with a photoionization term ( $W_{PI}$ ) and an avalanche term proportional with the intensity.  $N_0$  and  $N_e$  are the

density of atoms and the density of free carriers, respectively. The second term represents free carrier trapping and includes the term  $t_{tr}$ , corresponding to the free carrier trapping time (about 150 fs in pure SiO<sub>2</sub>) according to [7]. We have mentioned before that refinements of this equation were recently developed [26] based on electron energy considerations, leading to a correction of the avalanche term.

## 2.5 Energy relaxation and consequences on the refractive index

### 2.5.1 Introduction

In the last section, processes responsible for electronic excitation in transparent dielectrics with their respective contributions to the global free carrier generation have been reviewed. Via inverse bremsstrahlung, electromagnetic energy can be efficiently coupled to the free carrier gas and therefore significantly heat the electron bath. At the end of the femtosecond excitation sequence, the material is left in a state far from equilibrium where the lattice is still cold while free carriers play the role of an energetic reservoir. Relaxation processes start, converting the excess energy into structural alterations that can be sorted in two categories, point defects and matrix re-organization. Initiated by localized distortions of the lattice, point defects result in the creation of new molecular structures. In silica-based glasses, a change in the interconnectivity between SiO<sub>2</sub> tetrahedra leads to a matrix reorganization. Those processes obviously have consequences on the local density  $\rho$  and on the final polarizability  $\zeta$  (in cm<sup>3</sup>/mol) of the irradiated region. Those local modifications directly participate to the refractive index change according to the general refractivity formula [37]

$$\frac{n^2 - 1}{4\pi + b(n^2 - 1)} = \rho \frac{\zeta}{M}, \quad (2.35)$$

where  $M$  is the molar weight and  $b$  is a parameter depending on the overlap energy  $\Upsilon$

$$b = \frac{4\pi}{3} - \Upsilon. \quad (2.36)$$

Referring to [37],  $\Upsilon$  characterizes the overlapping degree of the electronic orbitals between the neighboring atoms in the solid. The parameter  $b$  is usually determined experimentally. When studying isolated atoms,  $\Upsilon$  vanishes and Eq. 2.35 reduces to the Lorentz-Lorenz formula.

## 2.5.2 Point defects

### Defect formation

A plethora of point defects is being inventoried since decades and their investigation has become an independent field of expertise regarding photochemical transformations. Defects can be transient, as distinct steps toward more stable arrangements or permanent. The appearance of point defects or color centers with a very defined optical signature is linked to the appearance of localized and discrete energy levels in the forbidden band, contributing thus to the overall absorption cross-section, but also to a local transformation, altering the optical, thermal, and mechanical properties of the material. Annealing in suitable conditions usually cancels those local inhomogeneities.

In pure fused silica glasses, the following scheme is generally adopted [1, 2].

The first step in the production of defects is the creation of a self trapped exciton (STE) [38]. Due to the strong polar character of interaction, an optically generated electron-hole pair (exciton) can localize itself on a site of the lattice. This localization spontaneously takes place for energetical reasons: the energy associated to a localized exciton is smaller than the one associated to a delocalized exciton and in despite of the energetical cost of the localization, the final energy variation is negative in  $\text{SiO}_2$ . This process invokes a local distortion of the lattice, notably a displacement of  $0.4 \text{ \AA}$  of the oxygen atom, stabilizing the exciton in return. Such an exciton is said to be self-trapped and is called a STE. Among its numerous signatures, STE's invoke a strong increase of the unit cell volume up to several tens of percent. STE's possess an absorption band at an energy of 2.8 eV, considerably enhancing the absorption properties of the material and therefore contributing greatly to cumulative effects. The creation of STE's in fused silica is extremely fast, about 150 fs according to Audebert and coworkers [7].

The release of this lattice distortion and of its associated quantity of energy results in breaking of the basic  $\text{SiO}_2$  tetrahedron and in the onset of point defects. For a pure fused silica glass, the decay of STE's translates into the formation of E' centers, non bridging hole centers (NBOHC), peroxy radicals and peroxy linkages, notably. The properties of those defects have been widely studied [1, 39, 40, 41, 42, 43]. A schematic representation of those defect structures with their associated absorption band is given in Fig. 2.2.

### Contribution of the point defects to the local refractive index alteration

For low densities of defects, the alteration of the real part of the refractive index can be predicted using a Drude model for the free electrons and a Lorentz model for the bound electrons, as proposed in [44]:

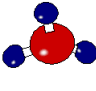
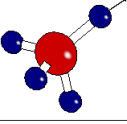
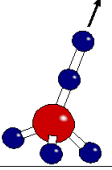
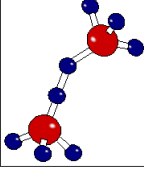
Defect	E'	NBOHC	Peroxy radical	Peroxy linkage
<b>Description</b> (• and / denote an unpaired electron)	$\equiv \text{Si} \cdot$ 	$\equiv \text{Si-O} \cdot$ 	$\equiv \text{Si-O-O} \cdot$ 	$\equiv \text{Si-O-O-Si} \equiv$ 
<b>Position in the bandgap</b> (with respect to the top of the valence band)	5.8 eV	2 eV	4.8-4.9 eV	

Figure 2.2: Principal points defects observed in fused silica [1, 2]. Large and small circles correspond to silicon and oxygen atoms, respectively.

$$n(\omega) = n_0 - \frac{N_e e^2}{2m_{vb}\epsilon_0\omega^2} + \sum_n \frac{N_n e^2}{2m_n\epsilon_0} \frac{1}{\omega_n^2 - \omega^2}, \quad (2.37)$$

where  $n_0$  is the refractive index of the pristine bulk,  $N_e$  and  $N_n$  are respectively the density of free and trapped electrons,  $e$  is the electron charge,  $m_{vb}$  is the optical mass an electron in the valence band,  $\epsilon_0$  is the dielectric constant of vacuum,  $\omega$  stands for the considered light frequency,  $\omega_n$  is the mean transition frequency of the trap labeled  $n$ , and  $m_n$  is the optical mass of an electron trapped on a  $n$ -type of defect. The contribution of a point defect to the global refractive index is positive for  $\omega_n > \omega$  and negative if  $\omega_n < \omega$ .

In permanent regime, the contributions of free electrons and transient defects vanish. Equation 2.37 can then be rewritten:

$$n(\omega) = n_0 - \sum_n \frac{N_n e^2}{2m_n\epsilon_0} \frac{1}{\omega_n^2 - \omega^2}. \quad (2.38)$$

Considering a unique type of defect with an intrinsic energy level located in the middle of the bandgap [41] (that is to say about 4.5 eV from the conduction band for fused silica), assuming that 1% of the initial  $\text{SiO}_2$  tetrahedra carry defects (i.e. for  $N_d = 2.2 \times 10^{19} \text{ cm}^{-3}$ ) and that the electron optical mass is about one half of the free electron mass, the resulting refractive index change is of about 0.1%. A refinement of this model taking into account additional terms is proposed in [45].

For more completeness, Kramers-Kronig analysis can be performed. This powerful method provides the spectral dependence of the induced refractive index change. Such results are presented in [46] in the frame of a molecular dynamics study. As a main difficulty, the Kramers-Kronig approach necessitates an in-depth knowledge of the absorption

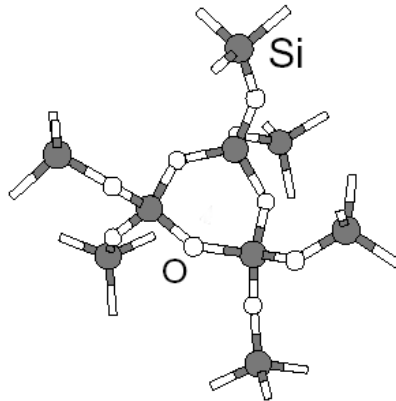


Figure 2.3: Example of a  $m$ -membered ring in fused silica with  $m = 3$ . Taken from [3]

spectrum of the photoinduced defects, preventing us from using it in the context of our experiments.

### 2.5.3 Matrix re-organization

In crystalline quartz transmission electron microscopy (TEM) analysis [47] clearly demonstrate that a field of stress appears in the vicinity of the interaction region. Another type of experimental work based on cleaving and topography study employing a phase shift interferometric microscope unambiguously shows a shear stress region located in the immediate neighborhood of the laser-written objects [48]. Those results suggest that the laser-affected material of higher refractive index than pristine bulk may have a higher density following a photophysical transformation [49].

Pristine amorphous fused silica is an assemblage of  $\text{SiO}_2$  tetrahedra. Those tetrahedra are linked together and form closed rings. The size of a ring is usually expressed in terms of number of Si-O segments, e.g. a 3- membered ring includes 3 Si-O segments, as shown in Fig. 2.3. Initially, the fused silica network is principally composed of 5- and 6- membered rings. Probing the effect of femtosecond laser irradiation, Raman spectroscopy studies [50] reveal a significant increase in the area of the peaks located at an energy near  $500 \text{ cm}^{-1}$  and  $600 \text{ cm}^{-1}$  in the laser-affected zone. Those peaks correspond to the onset of 3- and 4- membered rings, respectively, as established in [3]. Obviously, this drastic change in connectivity involves a dramatic drop in the average Si-O-Si bond angle and leads to the emergence of a more compact material. In addition to an increase of 3- membered rings, molecular dynamics simulations also report an increase in the number of large ring structures upon shockwave densification [51, 52]. Although the presence of large structures in a high density region may seem counterintuitive, Huang and Kieffer [53] underlined the higher



flexibility of large rings. Large structures (i.e. 8- or more membered rings) can fold up on themselves and therefore pack better as they are not constrained to keep a convex geometry.

Finally, an interesting connection between point defects and local densification is proposed in [54]. This model is based on the analysis of irradiated quartz and silica samples with different sources (neutrons, electrons, ions or photons). Surprisingly, the end products look very similar in terms of final density independently on the type of irradiation. Hence, Douillard and Duraud [54] suggest that densification of fused silica and quartz amorphization are provoked by a two-step mechanism. In a first step, point defects are induced, gradually accumulating stress in the glass matrix. A second step of structural relaxation is triggered when a critical density of about  $10^{18}$  E' point defects per gram is attained. This model, known as the Douillard-Duraud point defect model has been supported by recent molecular dynamics simulations [55].